Establishing ^{177}Lu-PSMA-617 Radioligand Therapy in a Syngeneic Model of Murine Prostate Cancer

Wolfgang P. Fendler[1], Andreea D. Stuparu[1], Susan Evans-Axelsson[1], Katharina Lückerath[1], Liu Wei[1], Woosuk Kim[1], Soumya Poddar[1], Jonathan Said[2], Caius G. Radu[1], Matthias Eiber[1], Johannes Czernin[1], Roger Slavik[1], and Ken Herrmann[1,3]

[1]*Department of Molecular and Medical Pharmacology, David Geffen School of Medicine at UCLA, Los Angeles, California;* [2]*Translational Pathology Core Laboratory, Department of Pathology and Laboratory Medicine, David Geffen School of Medicine at UCLA; and* [3]*Universitätsklinikum Essen, Department of Nuclear Medicine, Essen, Germany*

Clinical ^{177}Lu-PSMA-617 radioligand therapy (RLT) is applied in advanced-stage prostate cancer. However, to the best of our knowledge murine models to study the biologic effects of various activity levels have not been established. The aim of this study was to optimize specific and total activity for ^{177}Lu-PSMA-617 RLT in a syngeneic model of murine prostate cancer. **Methods:** Murine-reconstituted, oncogene-driven prostate cancer cells (0.1×10^6) (RM1), transduced to express human prostate-specific membrane antigen (PSMA), were injected into the left flank of C57Bl6 immunocompetent mice. RLT was performed by administering a single tail vein injection of ^{177}Lu-PSMA-617 at different formulations for specific (60 MBq at high, 62 MBq/nmol; intermediate, 31 MBq/nmol; or low 15 MBq/nmol specific activity) or total activity (30, 60, or 120 MBq). Organ distribution was determined by ex vivo γ-counter measurement. DNA double-strand breaks were measured using anti–gamma-H2A.X (phospho S139) immunohistochemistry. Efficacy was assessed by serial CT tumor volumetry and ^{18}F-FDG PET metabolic volume. Toxicity was evaluated 4 wk after the start of RLT. **Results:** Mean tumor-to-kidney ratios ± SEM were 19 ± 5, 10 ± 5, and 2 ± 0 for high, intermediate, and low (each $n = 3$) specific activity, respectively. Four of 6 (67%) mice treated with intermediate or high specific activity and none of 6 (0%) mice treated with low specific activity or formulation demonstrated significant DNA double-strand breaks (≥5% γ-H2A.X–positive cells). High when compared with intermediate or low specific activity resulted in a lower mean ± SEM tumor load by histopathology (vital tissue, 4 ± 2 vs. 8 ± 3 mm^2; $n = 3$ vs. 6), day-4 ^{18}F-FDG PET (metabolic volume, 87 ± 23 vs. 118 ± 14 mm^3; $n = 6$ vs. 12), and day-7 CT (volume, 323 ± 122 vs. 590 ± 46 mm^3; $n = 3$ vs. 6; $P = 0.039$). ^{177}Lu-PSMA-617 (120 MBq) with high specific activity induced superior tumor growth inhibition ($P = 0.021$, $n = 5$/group) without subacute hematologic toxicity ($n = 3$/group). **Conclusion:** ^{177}Lu-PSMA-617 (120 MBq) and high specific activity resulted in the highest efficacy in a syngeneic model of murine prostate cancer. The model will be useful for studying the effects of PSMA-directed RLT combined with potentially synergistic pharmacologic approaches.

Key Words: syngeneic; PSMA; prostate cancer; ^{177}Lu; specific activity

J Nucl Med 2017; 58:1786–1792
DOI: 10.2967/jnumed.117.193359

Prostate-specific membrane antigen (PSMA)–targeted radioligands have been introduced for treating patients with metastatic castrate-resistant prostate cancer (mCRPC) in several countries (*1–3*). The safety and effectiveness of ^{177}Lu-PSMA-617 radioligand therapy (RLT) are described in a recently published German multicenter study (*2*). Rahbar et al. reported a 50% decrease in serum prostate-specific antigen levels in about 50% and hematologic adverse events in only 12% of 145 patients after up to 4 cycles of ^{177}Lu-PSMA-617 (*2*). The high demand for this therapy led to the publication of first expert recommendations for clinical practice (*4*).

The clinical translation of PSMA-targeted RLT occurred before compound properties were published (*5,6*). Since then, ^{177}Lu-PSMA-617 RLT has been successfully performed in hundreds of prostate cancer patients worldwide. Given such rapid clinical translation, few attempts have been made to optimize radiation dose and specific activity for increased efficacy. Moreover, because PSMA-targeted RLT is not curative, synergistic pharmacologic approaches need to be identified.

Thus, there is a need to establish murine models of prostate cancer to permit optimization of RLT alone or in combination with drug treatments. Models should be based on immunocompetent mice to account for any effects of RLT on antitumor immune response. Here we report on an immunocompetent model of prostate cancer and investigate the impact of specific and total ^{177}Lu-PSMA-617 activity on organ distribution and RLT efficacy. The findings will help optimize ^{177}Lu-PSMA-617 RLT both for murine models and, potentially, for use in clinical routine or clinical trials to ultimately achieve better outcomes for mCRPC patients. Finally, the model will provide a platform to develop rational RLT protocols in combination with other therapeutic approaches.

MATERIALS AND METHODS

Cell Culture

RM1 carcinoma was previously induced by transfection of ras and myc oncogenes in reconstituted cells of C57BL/6 prostate origin (*7*). RM1 parental cells and RM1 cells stably transduced with human PSMA

Received Mar. 14, 2017; revision accepted May 15, 2017.
*For correspondence or reprints contact: Wolfgang Fendler, University of California at Los Angeles, Ahmanson Translational Imaging Division, 10833 Le Conte Ave., 200 Medical Plaza, Ste. B114-61, Los Angeles, CA 90095-7370.
E-mail: wfendler@mednet.ucla.edu
Published online May 25, 2017.

and SFG-Egfp/Luc (RM1-PGLS) were provided by Dr. Michel Sadelain (Memorial Sloan Kettering Cancer Center). A pMIY II-hPSMA plasmid was generated by the insertion of the human PSMA coding sequence into the multiple cloning site of the pMIY II (pMSCV-IRES-YFP II, Addgene 52108) plasmid. Amphotropic retroviruses were generated as previously described (*8*). To generate RM1-YFP and RM1-hPSMA lines, RM1 parental cells underwent transduction with the respective amphotropic retroviruses and were then sorted by flow cytometry to isolate pure populations of transduced cells. C4-2 cells were provided by Dr. George Thalmann (Department of Urology, Inselspital Bern). Cells were maintained in Dulbecco modified Eagle medium with 4.5 g/L glucose, L-glutamine (GIBCO), and 5% fetal bovine serum (ω-Scientific) and were grown at 37°C, 20% O_2, and 5% CO_2.

Flow Cytometry and PSMA Expression Level

Absolute numbers of PSMA proteins on the cell surface were quantified by flow cytometry based on mean fluorescence intensity values using the Quantum Simply Cellular (Bangs Laboratory) antihuman IgG quantification beads according to the manufacturer's instructions. PSMA was detected using allophycocyanin-labeled antihuman PSMA (clone REA408; Miltenyi Biotec). Briefly, 0.5×10^6 cells were incubated with the anti-PSMA antibody at a 1:5 dilution for 30 min at 4°C. Data were acquired on a 5 laser LSR II cytometer (BD). Data were analyzed using FlowJo (Three Star) software.

Mice

Male C57BL/6 or severe combined immunodeficiency mice were bred and housed under pathogen-free conditions. Studies were approved by the University of California at Los Angeles (UCLA) Animal Research Committee. The mice were 5–12 wk old at the onset of experiments. Four days before commencement of RLT, 0.1×10^6 tumor cells (RM1-hPSMA or RM1-PGLS) were injected subcutaneously into the shoulder region of C57BL/6 mice. C4-2 tumors were induced after subcutaneous injection of 5×10^6 cells in severe combined immunodeficiency mice.

Radiosynthesis

PSMA-617 precursor was obtained from ABX GmbH, and no-carrier-added $^{177}LuCl_3$ was obtained from ITG GmbH. The precursor was stored in aliquots (1 mg/mL) in 0.1% aqueous trifluoroacetic acid until use. For radiolabeling, 0.1 M sodium acetate buffer, pH 4.8, containing dihydroxybenzoic acid (10 mg/mL) was added to 1-, 2-, or 3-μg precursor and mixed with 60 MBq of $^{177}LuCl_3$ to obtain high (62 MBq/nmol), intermediate (31 MBq/nmol), or low (15 MBq/nmol) specific activity. The mixture was heated to 100°C for 30 min, diluted with phosphate-buffered saline, and sterilized by filtration. ^{177}Lu-PSMA-617 (30 and 120 MBq) was labeled at high (62 MBq/nmol) specific activity following the same protocol. Radiochemical purity was always greater than 99% without further purification.

Binding and Internalization Assay

Cells (10^5; triplicates in 24-well plates) were seeded and allowed to attach to the plate overnight. Cells were incubated with 4 nM ^{68}Ga-PSMA-11 in the absence or presence of 10 μM 2-(phosphonomethyl) pentane-1,5-dioic acid (PMPA) for 60 min at 37°C. Supernatant was collected, and cells were washed with glycine HCl, pH 2.8, to remove membrane-bound ligand. For collection of the internalized fraction, cells were lysed with 0.3N NaOH. Samples were measured in a γ-counter (Cobra II Auto-Gamma; Packard Instrument Co.).

For analysis of retention, cells were incubated with 4 nM ^{68}Ga-PSMA-11 for 60 min at 37°C and supernatant was collected. Cells were incubated in fresh medium for another 60 min in the absence or presence of 10 μM 2-(phosphonomethyl)pentane-1,5-dioic acid.

Decay-corrected data were expressed as percentage of bound, internalized, or retained radioligand, respectively, normalized to the total cell number.

Radioligand Therapy

Mice bearing subcutaneous RM1-hPSMA tumors were used to study specific activity in RLT (experiment 1; $n = 6$/group). RLT was started by administering a tail vein injection of formulation (no treatment [NT]) or 60 MBq of ^{177}Lu-PSMA-617 at high (62 MBq/nmol), intermediate (31 MBq/nmol), or low (15 MBq/nmol) specific activity. Animals were sacrificed at day 4 after the start of RLT for ^{177}Lu-PSMA-617 biodistribution and tissue analysis ($n = 3$/group; Fig. 1A) or were kept alive for tumor growth monitoring and survival ($n = 3$/group; Fig. 2A).

Mice bearing subcutaneous RM1-PGLS tumors were used to study total activity in RLT (experiment 2, $n = 5$/group). Animals were administered formulation (NT group) or 120, 60, or 30 MBq at high (62 MBq/nmol) specific activity and were kept alive for tumor growth monitoring and survival (Fig. 3A).

In experiment 3, RM1-hPSMA tumor–bearing mice were sacrificed at week 4 after administration of formulation (NT group) or 120, 60, or 30 MBq of ^{177}Lu-PSMA-617 at high (62 MBq/nmol) specific activity to assess subacute toxicity ($n = 3$/group).

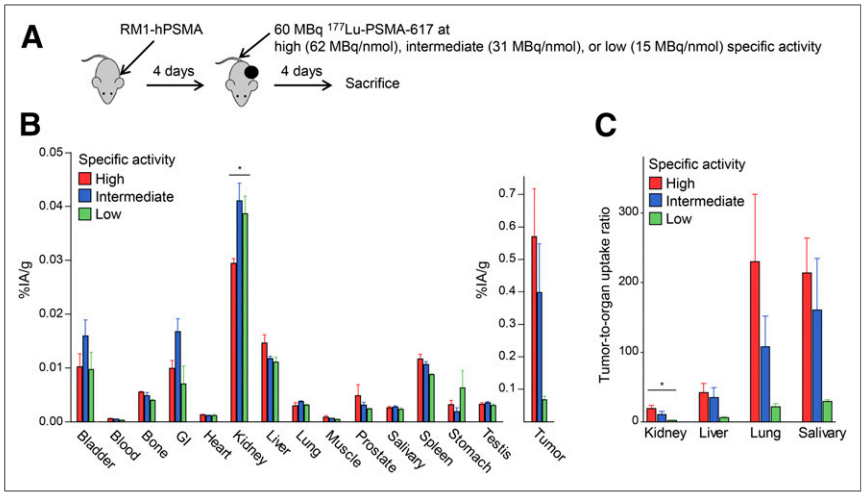

FIGURE 1. Biodistribution of ^{177}Lu-PSMA-617 at different levels of specific activity (experiment 1). (A) Mice received 60 MBq of ^{177}Lu-PSMA-617 at high (62 MBq/nmol), intermediate (31 MBq/nmol), or low (15 MBq/nmol) specific activity. Mice were sacrificed on day 4 to determine ^{177}Lu-PSMA-617 biodistribution (B) and tumor–to–organ uptake ratios (C). Data are mean %IA/g tissue + SEM ($n = 3$/group). Difference between high- versus intermediate- or low-specific-activity groups was assessed by Mann–Whitney test. *$P < 0.05$. GI = gastrointestinal tract.

PET/CT Image Acquisition

Baseline ^{68}Ga-PSMA-11 PET/CT was performed 2 d and baseline ^{18}F-FDG PET/CT was performed 1 d before the start of RLT to confirm PSMA expression and formation of viable tumor, respectively. Follow-up ^{18}F-FDG PET/CT was acquired on day 4. Tumor growth was monitored by serial CT acquisitions, 3 times per week until day 14 and 2 times per week thereafter.

Acquisition of static PET images commenced 60 min after application of 0.7–1.5 MBq of tracer using a preclinical PET/CT

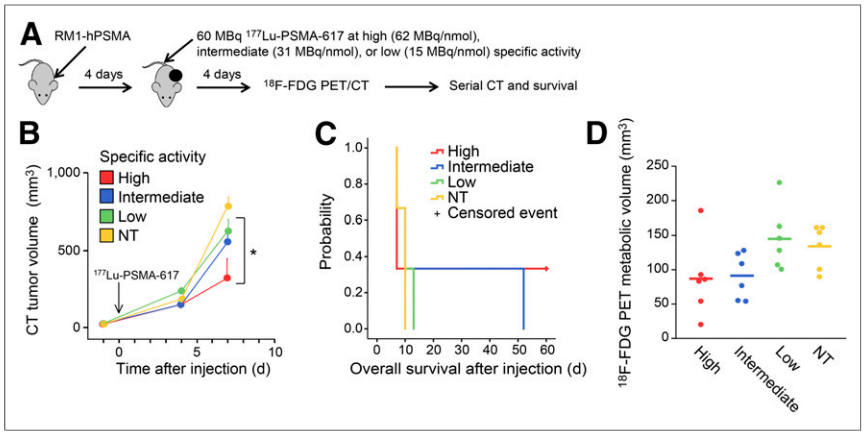

FIGURE 2. Response after ^{177}Lu-PSMA-617 RLT using high, intermediate, or low specific activity (experiment 1). (A) Mice received formulation (NT group) or 60 MBq of ^{177}Lu-PSMA-617 at high, intermediate, or low specific activity. CT tumor volume is shown until first animal per group was required to be sacrificed. Higher tumor uptake translates into more effective tumor growth inhibition (B, $*P = 0.039$), prolonged survival (C), and metabolic response (D). One mouse in high group had complete response and remained tumor free for more than 60 d (C). Difference between high- versus intermediate- to low-specific-activity groups was assessed by Mann–Whitney test. Data are presented as mean + SEM of $n = 3$ (B and C) or $n = 6$ (D) per group. $*P < 0.05$.

scanner (Genisys 8 PET/CT; Sofie Biosciences [successor of Genisys 4] (*9*)). Maximum-likelihood expectation maximization with 60 iterations was used for PET image reconstruction. All images were corrected for photon attenuation. The CT acquisition parameters were 40 kVp, 190 mA, and 720 projections with an exposure time of 55 ms at each projection.

PET/CT Image Analysis

PET/CT images were analyzed using OsiriX Imaging Software (version 3.9.3; Pixmeo SARL). The single reader was masked for specific and total ^{177}Lu-PSMA-617 activity.

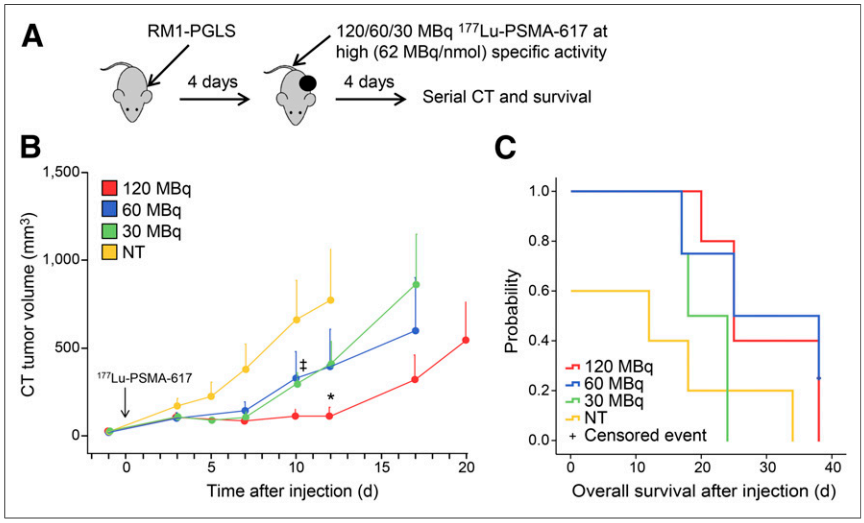

FIGURE 3. Tumor growth inhibition (A) and survival (B) after RLT using 30, 60, or 120 MBq of ^{177}Lu-PSMA-617 (experiment 2). (A) Mice received formulation (NT group) or 120, 60, or 30 MBq of ^{177}Lu-PSMA-617 at high specific activity. One hundred twenty MBq of ^{177}Lu-PSMA-617 induced most effective tumor growth inhibition (B, $*P = 0.021$) with improved survival (C). Difference between 120-MBq versus other groups was assessed by Mann–Whitney test on day 12. Data are mean + SEM of $n = 5$ per group. $*P < 0.05$; ‡1 mouse each died during PET/CT.

At baseline, PSMA expression and glucose metabolic activity were confirmed visually by focal uptake above background at the tumor cell injection site. To assess metabolic response, the ^{18}F-FDG PET volume was measured at baseline and follow-up using the Osirix region grow function to include all tumor voxels exceeding mean liver SUV plus 2 SDs, a definition proposed in the PERCIST (*10*).

For CT size measurements, entire tumors were delineated visually on more than 7 axial slices for each time point, and volume was calculated using the Osirix compute volume function.

Termination Criteria

Mice were sacrificed if tumor volume exceeded 1,000 mm^3 by caliper measurement or with the occurrence of skin ulcerations or other symptoms of deteriorating mouse condition. The UCLA Animal Research Committee protocol guidelines were applied. Caliper measurements were obtained by 1 masked investigator 3 times per week throughout the experiment and daily when tumors approached critical size.

Immunohistochemistry

Tumor sections were stained for γ-H2A.X (phospho S139), a marker of DNA double-strand breaks. Tissues were fixed overnight in 10% buffered formalin and transferred to 70% ethanol for storage. Paraffin-embedded samples were sectioned in the center of the tumor to obtain 4-μm slices. Paraffin was removed with xylene and rehydrated through graded ethanol. Endogenous peroxidase activity was blocked with 3% hydrogen peroxide in methanol for 10 min. Heat-induced antigen retrieval was performed for all sections in 0.01 M citrate buffer, pH 6.0, using a Biocare decloaker (Biocare Medical) at 95°C for 25 min. Primary rabbit polyclonal antigamma H2A.X (phospho S139) IgG (ab2893; Abcam) was added at 1:500 dilution in bovine serum albumin and incubated overnight at 4°C. Secondary staining was performed using the Dakocytomation Envision System labeled polymer horseradish peroxidase antirabbit (K4003; DakoCytomation, Carpinteria) and visualized with the diaminobenzidine reaction (#BDB2004 L; Biocare Medical) according to the manufacturer's instructions. The sections were counterstained with hematoxylin. All slides were mounted with Cytoseal (Fisher Scientific). Entire slides were scanned digitally at 40× using ScanScope AT (Leica Biosystems, Vista).

The area around the edges was disregarded to minimize influence of the edge effect. For visual analysis, a masked reader with prior immunohistochemistry experience delineated vital tumor tissue and categorized samples by percentage of γ-H2A.X–positive cells into negative, (+) 5%–10%, (++) 10%–20%, or (+++) >20%. For software analysis, high-resolution images of the entire section were diverted into brown nuclear

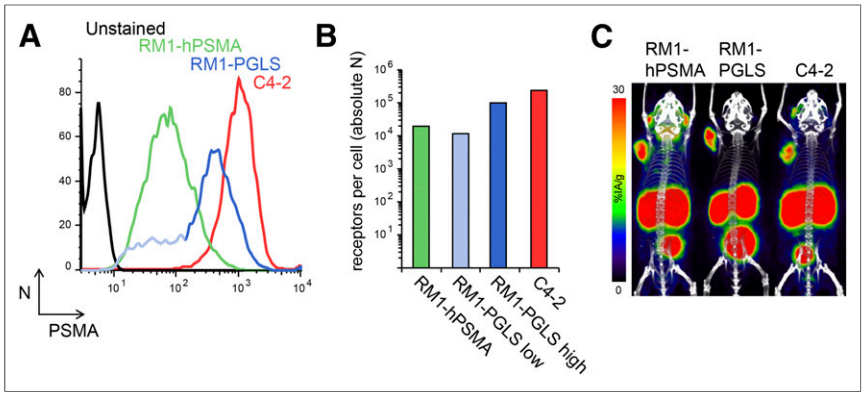

FIGURE 4. PSMA expression of mouse RM1 versus human C4-2 prostate cancer cell lines. (A) PSMA expression was determined in vitro by flow cytometry for RM1-hPSMA (green), RM1-PGLS (blue), and C4-2 (red). RM1-PGLS cells exhibit heterogeneous PSMA expression, with PSMA-low (light blue) and PSMA-high (dark blue) subpopulations. (B) Mean absolute numbers of PSMA on cell surface were quantified on basis of mean fluorescence intensity values using antihuman IgG quantification beads. (C) Representative ^{68}Ga-PSMA-11 PET/CT maximum-intensity projection of mice bearing equally sized subcutaneous mouse allografts or human xenografts. Mean %IA/g was 22.7, 17.4, and 15.5 for RM1-hPSMA, RM1-PGLS, and C4-2, respectively (n = 2 each).

staining for γ-H2A.X–positive cells and blue nuclear staining for γ-H2A.X–negative cells. ImageJ (version 1.51 g; National Institutes of Health) was used to count positive/negative cells greater than 15 μm in diameter.

Biodistribution and Toxicity

Biodistribution and toxicity were assessed in 2 separate experiments with 3 mice each. On day 4 after the start of RLT, the distributed ^{177}Lu-PSMA-617 activity was measured ex vivo in selected organs, tumor, and blood using a γ-counter. Uptake was expressed as percentage injected activity per gram of tissue (%IA/g).

Toxicity was assessed 4 wk after the start of RLT. Immediately after sacrifice, 100 μL or more of blood were drawn via cardiac puncture, and organs were inspected for any signs of deposits or damage. Blood analyses, including hemoglobin concentration, red and white blood cells, and platelets count, were performed using GENESIS Hematology Analyzer (Oxford Science).

Statistics

Data are presented as single values or mean ± SEM. Normal distribution of baseline variables was rejected by the Shapiro–Wilk test, and the Mann–Whitney test was used for unpaired comparison between 2 subgroups. Kaplan–Meier survival analysis was performed on the basis of the interval between the start of RLT and the date of sacrifice or the end of the experiment. Correlation was assessed using Spearman ρ. Significance was set at a P value of less than 0.05. The SPSS software package (version 15.0; SPSS, Inc.) was used for all statistical analysis.

RESULTS

Mouse (RM1) and Human (C4-2) Prostate Cancer Cells Demonstrate Similar PSMA Expression and Internalization In Vitro

PSMA expression was determined in vitro by flow cytometry for RM1-hPSMA, RM1-PGLS, and C4-2 (Fig. 4A). RM1-PGLS cells demonstrate heterogeneous expression with a smaller PSMA-low (mean fluorescence intensity, 44) and a larger PSMA-high subpopulation (mean fluorescence intensity, 466). PSMA expression was quantified on the basis of mean fluorescence intensity using antihuman IgG quantification beads. Median absolute PSMA numbers ranged from 19 × 10^3 (RM1-hPSMA) to 238 × 10^3 (C4-2, Fig. 4B) per cell. RM1-PGLS (56 × 10^3) and its PSMA-high subpopulation (99 × 10^3) demonstrated mean absolute PSMA numbers within 1 order of magnitude of C4-2. In vitro, ^{68}Ga-PSMA-11 cell surface binding and overall retention was highest for C4-2, and internalization was highest for RM1-PGLS with less than a 4-fold difference between the cell lines (Table 1). High uptake of ^{68}Ga-PSMA-11 was confirmed for all cell lines in vivo by PET/CT. Representative maximum-intensity-projection images of mice bearing equally sized subcutaneous RM1 allografts or C4-2 xenografts are shown in Figure 4C.

High Specific Activity Is Critical for High ^{177}Lu-PSMA-617 Tumor Uptake In Vivo (Experiment 1)

PSMA expression was confirmed by baseline ^{68}Ga-PSMA-11 PET/CT for all mice (Supplemental Fig. 1A; supplemental materials are available at http://jnm.snmjournals.org). RM1-hPSMA tumors were chosen for this experiment because of their homogeneous PSMA expression (Fig. 4A). To investigate the role of specific activity, RM1-hPSMA tumor–bearing mice (n = 6/group) received RLT as outlined in Figure 1A. Day-4 biodistribution and ^{177}Lu-PSMA-617 tumor–to–organ uptake ratios are shown in Figures 1B and 1C (n = 3/group). The kidneys had the highest organ uptake. Tumor uptake was higher (mean ± SEM, 0.57 ± 0.15 vs. 0.23 ± 0.10 %IA/g, P = 0.071) and kidney uptake was lower (0.03 ± 0.00 vs. 0.04 ± 0.00 %IA/g, P = 0.020) for high versus pooled low or intermediate specific activity (Fig. 1B). High specific activity resulted in highest tumor-to-kidney (mean ± SEM, 19 ± 5; P = 0.039), -liver (42 ± 13), -lung (230 ± 97), and –salivary gland (214 ± 50) ratios (Fig. 1C).

Higher ^{177}Lu-PSMA-617 Uptake Translates into More Severe DNA Damage and Tumor Growth Inhibition (Experiment 1)

Tumor tissue taken at day 4 was stained for γ-H2A.X by immunohistochemistry (n = 3/group). Representative images are shown in Figure 5A. RLT using intermediate or high specific activity induced significant DNA damage (≥5% positive cells) in 4 of 6 (67%) tumors both by visual and by software analysis (Figs. 5A and 5B). One of 3 (33%) tumors demonstrated significant DNA damage by visual analysis in mice that received low specific activity. In the NT group, all samples were negative (<5% positive cells).

On day 4, the mean ± SEM ^{18}F-FDG PET metabolic volume was 87 ± 23 (high), 91 ± 14 (intermediate), 145 ± 19 (low), and 134 ± 13 mm^3 (NT; n = 6/group, Fig. 2D). The area of vital tumor tissue was 4 ± 2 (high), 4 ± 1 (intermediate), 12 ± 6 (low), and 7 ± 1 mm^2 (NT, n = 3/group, Supplemental Fig. 3A). Metabolic volume correlated significantly with the area of vital tumor tissue (P < 0.01, Spearman ρ = 0.73; Supplemental Fig. 3B), despite 1 outlier in the low group.

TABLE 1
Mouse and Human Prostate Cancer Cell Surface Binding, Internalization, and Retention of ^{68}Ga-PSMA-11

Cell line	Surface binding (%IA per 10^5 cells)	Internalization (%IA per 10^5 cells)	Retention (%IA per 10^5 cells)
Mouse			
RM1-hPSMA	2.3 ± 0.3	6.8 ± 0.2	5.1 ± 0.3
RM1-PGLS	4.4 ± 0.3	9.9 ± 0.2	3.1 ± 0.6
Human			
C4-2	7.4 ± 0.3	6.7 ± 0.2	8.6 ± 1.4

Data are mean %IA ± SEM of $n = 3$ per group; representative of 2 independent experiments.

High specific activity resulted in significantly lower mean ± SEM CT tumor volume at day 7 (323 ± 122 mm^3) when compared with intermediate or low specific activity (590 ± 46 mm^3, $P = 0.039$, $n = 3$/group; Fig. 2B). Kaplan–Meier curves demonstrated a survival of more than 50 d for 1 each mouse in the high and intermediate groups ($n = 3$/group; Fig. 2C).

120 MBq of ^{177}Lu-PSMA-617 Induced Most Efficient Tumor Growth Inhibition (Experiment 2)

High specific activity was associated with high efficacy. On the basis of a more consistent tumor growth (Supplemental Fig. 2), RM1-PGLS–bearing mice were chosen for experiment 2. To investigate the impact of total activity, RM1-PGLS–bearing mice received formulation (NT group) or RLT at 3 different activity levels (30, 60, or 120 MBq; $n = 5$/group), each at high specific activity (Fig. 3A). Mice that received 120 and 60 MBq of ^{177}Lu-PSMA-617 survived longer than animals that received 30 MBq or NT (Fig. 3C). One hundred twenty megabecquerels induced the most efficient tumor growth inhibition as determined by serial CT ($P = 0.021$). The mean ± SEM tumor volume on day 12 was 113 ± 50 (120 MBq), 393 ± 214 (60 MBq), 412 ± 127 (30 MBq), and 774 ± 291 mm^3 (NT, Fig. 3B).

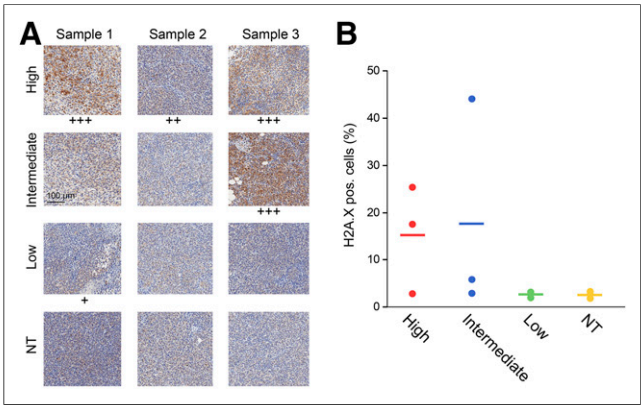

FIGURE 5. DNA damage induced by ^{177}Lu-PSMA-617 RLT using high, intermediate, or low specific activity (experiment 1). (A) Representative areas of tumor tissue stained for γ-H2A.X are shown at 10-fold magnification (conditions in separate rows). Proportion of γ-H2A.X–positive cells was evaluated by a masked reader visually (A) and by ImageJ software (B). + = 5%–10%; ++ = 10%–20%; +++ = >20% γ-H2A.X–positive cells. Dots represent single values; bars are mean values ($n = 3$ per group).

120 MBq of ^{177}Lu-PSMA-617 Was Safe (Experiment 3)

To evaluate toxicity, RM1-hPSMA–bearing mice received formulation (NT group) or RLT with 30, 60, or 120 MBq of ^{177}Lu-PSMA-617 ($n = 3$ each) at high specific activity. Four weeks after the start of RLT, none of the mice demonstrated pathologic findings on gross examination with reference to organ size, shape, color, and texture. The mean hemoglobin concentration, red and white blood cell counts, and platelet numbers were within reference range for each group (Fig. 6).

DISCUSSION

Here we established a syngeneic mouse model of prostate cancer aimed at optimizing specific and total activity levels for ^{177}Lu-PSMA-617 RLT. We selected 3 specific activity levels based on clinical ^{177}Lu-PSMA-617 RLT protocols (*2*) and 3 total activity levels established in mouse models of somatostatin receptor–targeted RLT (*11*). High specific activity was associated with the highest tumor uptake and more prominent DNA damage. Mice that received 120 MBq of ^{177}Lu-PSMA-617 RLT with high specific activity displayed no adverse health effects throughout the study and had hemoglobin and blood count levels within a safe range at 4 wk after injection. One hundred twenty megabecquerels of ^{177}Lu-PSMA-617 RLT also resulted in the most effective tumor growth inhibition. RM1-based cells used in our studies demonstrate similar PSMA expression, internalization and retention when compared with human prostate cancer cells in vitro. This mouse model can now be used to test rationally designed combination therapies.

Our findings have implications for clinical and preclinical ^{177}Lu-PSMA-617 RLT. First, the critical role of high specific activity for ^{177}Lu-PSMA-617 was established for tumor–to–organ uptake ratios of the radioligand. More important, high specific activity was associated with high levels of DNA double-strand break, determined by γ-H2A.X staining, a prerequisite for effective tumor growth inhibition. The range of specific activity tested in our mouse model was representative of clinical protocols. Twelve centers reported specific activity for a total of 123 ^{177}Lu-PSMA-617 RLT applications in mCRPC patients (*2*). Specific activity within the German dataset ranged from 23 to 78 MBq/nmol (mean, 48 MBq/nmol; written personal correspondence with Bernd Krause from the German Society of Nuclear Medicine) matching our experiment parameters (range, 15–62 MBq/nmol). Improved tumor uptake by high specific activity is in line with previous findings for a similar compound (PSMA-I&T) labeled with ^{111}In (*12*).

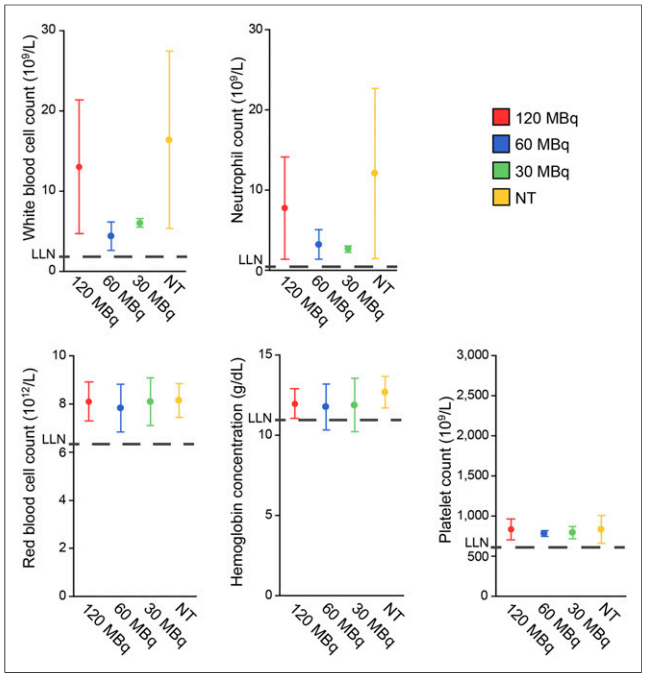

FIGURE 6. Hemoglobin and blood count level 4 wk after RLT using 30, 60, or 120 MBq of ^{177}Lu-PSMA-617 (experiment 3). ^{177}Lu-PSMA-617 RLT was not associated with relevant hematotoxicity. Data are mean ± SEM of n = 3/group. LLN = lower limit of reference range.

Our findings suggest that the use of intermediate- or low-specific-activity ^{177}Lu-PSMA-617, as reported previously (*13*), may be suboptimal. A comparison of different specific activity levels is important, given prior reports of improved tumor–to–organ uptake for other radiolabeled compounds, including ^{68}Ga-OPS202/^{177}Lu-OPS201 (*14*) and ^{90}Y-ibritumomab (*15*).

Furthermore, mouse data on safety and efficacy of different activity levels are now available for future evaluation. Of the 3 total activity levels assessed in this study (30, 60, and 120 MBq), 120 MBq of ^{177}Lu-PSMA-617 resulted in the most effective tumor growth inhibition. One hundred twenty megabecquerels of ^{177}Lu-PSMA-617 did not result in subacute or life-threatening bone marrow toxicity. Radiation nephropathy, a late event previously reported after application of ^{90}Y-labeled radioligands (*16*), was not analyzed in these experiments given the short median survival of 25–32 d after the start of therapy and the lack of accurate early biomarkers.

^{177}Lu-PSMA-617 RLT is safe and effective in patients with mCRPC. Biochemical response was documented in about half of patients undergoing ^{177}Lu-PSMA-617 RLT (*2*). RLT is well tolerated, with low rates (<15%) of grade 3–4 hematologic adverse events (*2*), and no relevant kidney toxicity has been documented thus far (*1,2,17–20*). However, ^{177}Lu-PSMA-617 RLT alone is not curative. Therefore, rational combination of ^{177}Lu-PSMA-617 RLT with other synergistic therapies, including immunotherapy, will help to improve outcomes for mCRPC patients. Our model can be used for this purpose.

Our study has several limitations. We observed shrinkage of RM1-hPSMA tumors starting from day 14 after inoculation in about one third of untreated C57Bl6 mice (Supplemental Fig. 2). Adaptive immune response was indicated by a tumor rechallenge experiment using PSMA-positive (RM1-hPSMA, RM1-PGLS) and PSMA-negative (RM1-YFP) cell lines (Supplemental Fig. 4). Adaptive immune response directed at human PSMA poses a limitation of the RM1-hPSMA cells with high expression level for PSMA. Tumor rejection was not seen for RM1-PGLS cells with heterogeneous PSMA expression (Fig. 4A).

CONCLUSION

We established ^{177}Lu-PSMA-617 RLT in a syngeneic model of murine prostate cancer. In vitro, RM1 murine cell lines were similar to human prostate cancer cells in terms of PSMA expression, internalization, and retention. In vivo, high specific activity was critical for optimal tumor growth inhibition. Up to 120 MBq of ^{177}Lu-PSMA-617 was applied without relevant subacute toxicity. Long-term toxicity was not evaluated. This model will serve future evaluation of combination therapy with potentially synergistic pharmacologic approaches.

DISCLOSURE

This study was partially funded by the U.S. Department of Energy, Office of Science Award (DE-SC0012353), and UCLA SPORE in Prostate Cancer (P50 CA092131). Wolfgang P. Fendler and Katharina Lückerath each received a scholarship from the German Research Foundation (Deutsche Forschungsgemeinschaft, DFG, grants 807122 and 807454, respectively). Susan Evans-Axelsson was supported by the Swedish Research Council International Postdoc Grant (grant number 2015-00452). Caius G. Radu and Johannes Czernin are cofounders of Sofie Biosciences. No other potential conflict of interest relevant to this article was reported.

ACKNOWLEDGMENTS

We thank Larry Pang for his assistance with PET/CT imaging studies and Ngan Doan for help with immunohistochemistry. We acknowledge the UCLA Biomedical Cyclotron for producing the PET probes used in this study. We thank Bernd Krause and the German Society of Nuclear Medicine ^{177}Lu-PSMA-617 consortium for access to human data.

REFERENCES

1. Yadav MP, Ballal S, Tripathi M, et al. ^{177}Lu-DKFZ-PSMA-617 therapy in metastatic castration resistant prostate cancer: safety, efficacy, and quality of life assessment. *Eur J Nucl Med Mol Imaging.* 2017;44:81–91.
2. Rahbar K, Ahmadzadehfar H, Kratochwil C, et al. German multicenter study investigating ^{177}Lu-PSMA-617 radioligand therapy in advanced prostate cancer patients. *J Nucl Med.* 2017;58:85–90.
3. Demir M, Abuqbeitah M, Uslu-Besli L, et al. Evaluation of radiation safety in ^{177}Lu-PSMA therapy and development of outpatient treatment protocol. *J Radiol Prot.* 2016;36:269–278.
4. Fendler WP, Kratochwil C, Ahmadzadehfar H, et al. ^{177}Lu-PSMA-617 therapy, dosimetry and follow-up in patients with metastatic castration-resistant prostate cancer. *Nuklearmedizin.* 2016;55:123–128.
5. Benešová M, Schafer M, Bauder-Wust U, et al. Preclinical evaluation of a tailor-made DOTA-Conjugated PSMA inhibitor with optimized linker moiety for imaging and endoradiotherapy of prostate cancer. *J Nucl Med.* 2015;56:914–920.
6. Kratochwil C, Giesel FL, Eder M, et al. ^{177}Lu lutetium-labelled PSMA ligand-induced remission in a patient with metastatic prostate cancer. *Eur J Nucl Med Mol Imaging.* 2015;42:987–988.
7. Thompson TC, Southgate J, Kitchener G, Land H. Multistage carcinogenesis induced by ras and myc oncogenes in a reconstituted organ. *Cell.* 1989;56:917–930.

8. Kim W, Le TM, Wei L, et al. [^{18}F]CFA as a clinically translatable probe for PET imaging of deoxycytidine kinase activity. *Proc Natl Acad Sci USA.* 2016;113:4027–4032.
9. Herrmann K, Dahlbom M, Nathanson D, et al. Evaluation of the Genisys4, a bench-top preclinical PET scanner. *J Nucl Med.* 2013;54:1162–1167.
10. Wahl RL, Jacene H, Kasamon Y, Lodge MA. From RECIST to PERCIST: evolving considerations for PET response criteria in solid tumors. *J Nucl Med.* 2009;50:122S–150S.
11. Svensson J, Molne J, Forssell-Aronsson E, Konijnenberg M, Bernhardt P. Nephrotoxicity profiles and threshold dose values for [^{177}Lu]-DOTATATE in nude mice. *Nucl Med Biol.* 2012;39:756–762.
12. Chatalic KL, Heskamp S, Konijnenberg M, et al. Towards personalized treatment of prostate cancer: PSMA I&T, a promising prostate-specific membrane antigen-targeted theranostic agent. *Theranostics.* 2016;6:849–861.
13. Chakraborty S, Chakravarty R, Shetty P, Vimalnath KV, Sen IB, Dash A. Prospects of medium specific activity ^{177}Lu in targeted therapy of prostate cancer using ^{177}Lu-labeled PSMA inhibitor. *J Labelled Comp Radiopharm.* 2016;59:364–371.
14. Nicolas GP, Mansi R, Kaul F, et al. ^{68}Ga-OPS202/^{177}Lu-OPS201, a high performance theranostic pair of radiolabelled somatostatin antagonists for PET imaging and radionuclide therapy: translational aspects. *Eur J Nucl Med Mol Imaging.* 2015;42:129.
15. Knox SJ, Goris ML, Trisler K, et al. Yttrium-90-labeled anti-CD20 monoclonal antibody therapy of recurrent B-cell lymphoma. *Clin Cancer Res.* 1996;2:457–470.
16. Villard L, Romer A, Marincek N, et al. Cohort study of somatostatin-based radiopeptide therapy with [^{90}Y-DOTA]-TOC versus [^{90}Y-DOTA]-TOC plus [^{177}Lu-DOTA]-TOC in neuroendocrine cancers. *J Clin Oncol.* 2012;30:1100–1106.
17. Fendler WP, Reinhardt S, Ilhan H, et al. Preliminary experience with dosimetry, response and patient reported outcome after ^{177}Lu-PSMA-617 therapy for metastatic castration-resistant prostate cancer. *Oncotarget.* 2017;8:3581–3590.
18. Kratochwil C, Giesel FL, Stefanova M, et al. PSMA-targeted radionuclide therapy of metastatic castration-resistant prostate cancer with ^{177}Lu-labeled PSMA-617. *J Nucl Med.* 2016;57:1170–1176.
19. Rahbar K, Schmidt M, Heinzel A, et al. Response and tolerability of a single dose of ^{177}Lu-PSMA-617 in patients with metastatic castration-resistant prostate cancer: a multicenter retrospective analysis. *J Nucl Med.* 2016;57:1334–1338.
20. Ahmadzadehfar H, Eppard E, Kurpig S, et al. Therapeutic response and side effects of repeated radioligand therapy with ^{177}Lu-PSMA-DKFZ-617 of castrate-resistant metastatic prostate cancer. *Oncotarget.* 2016;7:12477–12488.